

## Defining the molecular evolution of extrauterine high grade serous carcinoma

James P. Beirne<sup>a, c, \*</sup>, Darragh G. McArt<sup>b</sup>, Aideen Roddy<sup>b</sup>, Clara McDermott<sup>a</sup>, Jennifer Ferris<sup>a</sup>, Niamh E. Buckley<sup>a, d</sup>, Paula Coulter<sup>d</sup>, Nuala McCabe<sup>a</sup>, Sharon L. Eddie<sup>a</sup>, Philip D. Dunne<sup>e</sup>, Paul O'Reilly<sup>b</sup>, Alan Gilmore<sup>b</sup>, Laura Feeney<sup>a, g</sup>, David Lyons Ewing<sup>a</sup>, Ronny I. Drapkin<sup>f</sup>, Manuel Salto-Tellez<sup>a, h</sup>, Richard D. Kennedy<sup>a, g</sup>, Ian J.G. Harley<sup>a, c</sup>, W. Glenn McCluggage<sup>a, c, i</sup>, Paul B. Mullan<sup>a</sup>

<sup>a</sup> Ovarian Cancer Research Programme, Centre for Cancer Research and Cell Biology, Queen's University, Belfast, United Kingdom of Great Britain and Northern Ireland

<sup>b</sup> Department of Cancer Bioinformatics, Queen's University, Belfast, United Kingdom of Great Britain and Northern Ireland

<sup>c</sup> Northern Ireland Centre for Gynaecological Cancer, Belfast Health and Social Care Trust, Belfast, United Kingdom of Great Britain and Northern Ireland

<sup>d</sup> School of Pharmacy, Queen's University, Belfast, United Kingdom of Great Britain and Northern Ireland

<sup>e</sup> Department of Translational Cancer Genomics, Centre for Cancer Research and Cell Biology, Queen's University, Belfast, United Kingdom of Great Britain and Northern Ireland

<sup>f</sup> Ovarian Cancer Research Center, University of Pennsylvania Perelman School of Medicine, Philadelphia, PA, USA

<sup>g</sup> Northern Ireland Cancer Centre, Belfast Health and Social Care Trust, Belfast, United Kingdom of Great Britain and Northern Ireland

<sup>h</sup> Northern Ireland Molecular Pathology Laboratory, Centre for Cancer Research and Cell Biology, Queens University, Belfast, United Kingdom of Great Britain and Northern Ireland

<sup>i</sup> Department of Pathology, Belfast Health and Social Care Trust, Belfast, United Kingdom of Great Britain and Northern Ireland

### H I G H L I G H T S

- New molecular evidence that high grade serous carcinogenesis commences in the distal fallopian tube.
- Serous tubal intra-epithelial carcinoma is molecularly highly similar to metastatic high grade serous carcinoma.
- Aberrant upregulation of mitosis-related pathways is strongly associated with evolution of HGSC from the fallopian tube.

### A R T I C L E I N F O

#### Article history:

Received 1 May 2019

Received in revised form 23 August 2019

Accepted 25 August 2019

Available online 4 September 2019

#### Keywords:

Ovarian cancer

Pathogenesis

Molecular profiling

### A B S T R A C T

**Objective:** High grade serous carcinoma (HGSC) is the most common and most aggressive, subtype of epithelial ovarian cancer. It presents as advanced stage disease with poor prognosis. Recent pathological evidence strongly suggests HGSC arises from the fallopian tube via the precursor lesion; serous tubal intraepithelial carcinoma (STIC). However, further definition of the molecular evolution of HGSC has major implications for both clinical management and research. This study aims to more clearly define the molecular pathogenesis of HGSC.

**Methods:** Six cases of HGSC were identified at the Northern Ireland Gynaecological Cancer Centre (NIGCC) that each contained ovarian HGSC (HGSC), omental HGSC (OMT), STIC, normal fallopian tube epithelium (FTE) and normal ovarian surface epithelium (OSE). The relevant formalin-fixed paraffin embedded (FFPE) tissue samples were retrieved from the pathology archive via the Northern Ireland Biobank following attaining ethical approval (NIB11:005).

Full microarray-based gene expression profiling was performed on the cohort. The resulting data was analysed bioinformatically and the results were validated in a HGSC-specific in-vitro model.

**Results:** The carcinogenesis of HGSC was investigated and showed the molecular profile of HGSC to be more closely related to normal FTE than OSE. STIC lesions also clustered closely with HGSC, indicating a common molecular origin.

**Conclusion:** This study provides strong evidence suggesting that extrauterine HGSC arises from the fimbria of the distal fallopian tube. Furthermore, several potential pathways were identified which could

\* Corresponding author at: Centre for Cancer Research and Cell Biology, Queen's University, 97 Lisburn Road, Belfast BT9 7AE, United Kingdom of Great Britain and Northern Ireland.  
E-mail address: [j.beirne@qub.ac.uk](mailto:j.beirne@qub.ac.uk) (J.P. Beirne).

be targeted by novel therapies for HGSC. These findings have significant translational relevance for both primary prevention and clinical management of the disease.

© 2019 Elsevier Inc. All rights reserved.

## 1. Introduction

Epithelial ovarian cancer (EOC) is the most lethal gynaecological malignancy in the western world. In 2012 there were 152,000 and 4300 deaths from ovarian cancer worldwide and in the UK, respectively [1]. This equates to twelve women dying from ovarian cancer daily within the UK. High grade serous carcinoma (HGSC) accounts for ~70% of all EOCs and ~90% of advanced stage EOCs (stage III-IV), making it the most common and most deadly subtype.

At a molecular level, HGSC is essentially ubiquitous for *p53* mutations [2]. Germline mutations in the *BRCA1* or *BRCA2* genes are present in 6.5–19% of HGSCs [3]. *BRCA*-mutated HGSCs are associated with an increased likelihood of visceral metastases [4]. *BRCA1* dysfunction is also detected in sporadic cases with mutations reported in 15–72% and loss of function (*BRCAness*) observed at high frequency [5,6].

Despite extensive investigation, the molecular mechanisms of HGSC development remain unknown. Historically, it was thought HGSC developed from the ovarian surface epithelium (OSE) due to errors in cell replication associated with the repair of trauma incurred by ovulation [7]. Several epidemiological studies supported this theory with evidence that women with an increased number of lifetime ovulations are at a greater risk of developing HGSC [8–11].

Recently, pathological evidence has emerged that supports the theory that the distal fallopian tube is the origin of HGSC [12]. Initial evidence for a tubal origin came from the study of risk-reducing salpingo-oophorectomy (RRSO) specimens in women at high risk of hereditary breast and ovarian cancers [13,14]. Further investigation revealed most HGSCs arise from the distal fallopian tube from a precursor referred to as serous tubal intraepithelial carcinoma (STIC) [15]. These STIC lesions show identical *p53* mutations to the adjacent HGSC establishing a link between STIC and HGSC [16]. To complement this pathological data, we now present strong molecular evidence suggesting high grade serous carcinogenesis commences in the fallopian tube.

## 2. Materials and methods

### 2.1. Study cohort and tissue preparation

Tissue samples from six cases of sporadic, stage III/IV HGSC were collected from patients who underwent primary cytoreductive surgery at the Northern Ireland Gynaecological Cancer Centre (Ethical approval: Northern Ireland Biobank NIB11:005, NIB13:0094). Cases were chosen based on the availability of the following tissues: normal OSE, normal FTE, STIC, ovarian HGSC, and OMT. All cases had fully anonymised, matched clinico-pathological data (see Supplementary file 1).

A haematoxylin and eosin (H&E) stained slide was prepared from each formalin fixed paraffin embedded (FFPE) block from all six cases. The slides were reviewed by a specialist Gynaecological Pathologist (WGM) and appropriate areas annotated for each of the five sample sites. The STIC lesions were selected from an area distant from tumour to minimise contamination. Subsequently, ten 5 µm sections were cut for macrodissection and RNA preparation. Finally, a further H&E was prepared to confirm the annotated regions were still present and therefore represented throughout the sections for RNA preparation.

### 2.2. RNA preparation and gene expression profiling

RNA was extracted using the Roche HighPure® RNA Isolation Kit (Roche, UK). Following RNA extraction, spectrophotometer quality control (QC) was performed. All samples were amplified using the WT-Ovation FFPE System V2 kit (NuGEN Technologies Inc., San Carlos, CA, USA). Following amplification, cDNA samples were quality controlled using both the spectrophotometer and the Agilent 2100 bioanalyzer. Samples proceeded to fragmentation and labelling using the NuGEN Encore Biotin module V2 (NuGEN Technologies Inc.), before hybridisation onto Xcel® arrays (ALMAC Diagnostics, Craigavon, UK) in accordance with the NuGEN guidelines for hybridisation onto Affymetrix GeneChip® arrays.

### 2.3. Bioinformatic analysis

Background correction and normalization of gene expression data was carried out using *justRMA*, provided by the 'affy' Bioconductor package [17], within the R statistical package (version 3.2.2) [18]. Initial correspondence analysis was carried out on all the samples using the 'ade4' [19] and 'made4' [20] packages. Both the complete expression set and a non-specific variance based filtered expression set implemented by the 'genefilter' [21] package, retaining the top twenty percent of most variant probes, were analysed.

Following initial analysis, three comparisons (FTE vs. STIC, STIC vs. ovarian HGSC and ovarian HGSC vs. OMT) were performed, using *genefilter* to rank the probes on the F-test and assessed the top one hundred probes ability to stratify by way of a heatmap derived from a hierarchical clustering method involving squared Euclidean distance and Ward's method, as described by Murtagh and Legendre [22], using the 'heatmap.plus' [23] package. The *limma* package [24] was then used to identify the top differentially expressed genes for each comparison. These gene lists were uploaded to Ingenuity Pathway Analysis (IPA®, QIAGEN Redwood City, [www.qiagen.com/ingenuity](http://www.qiagen.com/ingenuity)) according to their Ensembl ID, with a false discovery rate cut off set at 0.05. A core analysis was performed on each of the data sets using the parameters outlined in Supplementary file 2.

The analysis assessed the activity of canonical pathways within the dataset, based on the z-score. An orange bar means the analysis software predicted an overall increase in the activity of the pathway, a blue bar means the software predicted an overall decrease in the activity of the pathway, a white bar means that pathway activity is unchanged from normal, and a grey bar means that activity predictions were not possible (mainly due to a lack of publications in the topic area). The ratio of pathway activity is identified by the orange line. From these analyses, the top ten canonical pathways were identified for each of the three comparisons. Subsequently, gene expression profiles from an independent HGSC dataset were downloaded from the NCBI Gene Expression Omnibus (<http://www.ncbi.nlm.nih.gov/geo/>) under accession number GSE69429. This dataset contained transcription profiles of normal fallopian tube, STIC and HGSC from 6 patients (n = 18 samples in total). The transcriptional profiles were generated on the Affymetrix HuEx-1\_0-st-v2 array. We utilised the core gene normalised series matrix data for the analysis in our study.

The top 500 differentially expressed genes/probes representing the FTE vs. STIC and STIC vs. ovarian HGSC comparisons, from our

study, were filtered to include genes/probes which had an adjusted  $p$ -value  $< 0.05$  and fold change  $\pm 1.5$ . This generated two filtered gene lists; STIC vs ovarian HGSC reduced to 79 transcripts encoding 51 unique genes and FTE vs STIC reduced to 154 transcripts encoding 103 unique genes.

Partek Genomics Suite software (version 6.6) (Partek Inc., St. Louis, MO, USA.) was used for analysis of the independent dataset. For clustering, data matrices were standardised to the median value of probe sets expression. Standardisation of the data allows for comparison of expression levels for different probe sets. Following standardisation, 2-dimensional hierarchical clustering was performed. Euclidean distance was used to calculate the distance matrix; a multidimensional matrix representing the distance from each data point (probe set-sample pair) to all the other data points. Ward's linkage method was subsequently applied to join samples and genes together, with the minimum variance, to find compact clusters based on the calculated distance matrix.

#### 2.4. *In vitro* validation model

A HGSC-specific cell model was curated from validated cell lines [25,26]. KURAMOCHI, OVCAR3 and OVCAR4 were maintained in RPMI supplemented with 10% fetal calf serum (FCS), 1 mmol/L sodium pyruvate, and 50  $\mu\text{g}/\text{mL}$  penicillin-streptomycin (Life Technologies Inc., UK.) COV362 were maintained in DMEM supplemented with 10% FCS, 1 mmol/L sodium pyruvate, and 50  $\mu\text{g}/\text{mL}$  penicillin-streptomycin (Life Technologies Inc., UK.).

A non-HGSC specific cell model was also curated from validated cell lines [25,26]. IGROV1 and SKOV3 were maintained in RPMI with 10% FCS, 1 mmol/L sodium pyruvate, and 50  $\mu\text{g}/\text{mL}$  penicillin-streptomycin (Life Technologies Inc., UK.). JHOC5 were maintained in DMEM/F12, 10% FCS and 0.1  $\mu\text{M}$  NEAA.

Fallopian tube secretory epithelial cells (FTSECs) were obtained from one of the authors (RID) [27]. FT190 was used to represent normal FTE and FT246 (containing a stable p53 shRNA construct) was used to represent STIC. They were maintained in DMEM-Ham's F12 (Gibco®, Thermo Fisher Scientific Inc., UK) 2% Ultrosor G (Pall BioSeptra, Cergy, France) and 1% penicillin-streptomycin (Life Technologies Inc., UK) [27]. Total RNA was extracted using RNA STAT60® (Invitrogen) and quantified using the NanoDrop 2000 spectrophotometer (Thermo Fisher Scientific Inc., UK.). Subsequently, 2  $\mu\text{g}$  RNA was reverse transcribed using the Transcriptor First Strand cDNA Synthesis Kit (Roche, UK).

#### 2.5. FFPE tissue validation model

The RNA preparation procedure described above was repeated in the six-patient cohort, within the Northern Ireland Molecular Pathology Laboratory (NIMPL). Total RNA was quantified using the QUBIT fluorometer (Thermo Fisher Scientific Inc., UK.). Subsequently, 0.5  $\mu\text{g}$  RNA was reverse transcribed using the Transcriptor First Strand cDNA Synthesis Kit (Roche, UK).

#### 2.6. Endonuclease-prepared siRNA screening strategy

The Mission® esiRNA platform (Sigma-Aldrich, Dorset, UK) was used to design an assay containing 60 esiRNAs (58 targets and 2 controls) against several potential oncogenic targets. The selection was based upon the GEP data along with inclusion of some commonly known oncogenes (see Supplementary file 3). R-luciferase (R-LUC) and KIF11 were selected as negative and positive controls respectively. This platform was selected to reduce the likelihood of any identified effect on cell viability being associated

with off-target effects. The esiRNA screen was performed using a cell density of 2000/well in a 96-well plate with an incubation of 7 days, in triplicate (FT190, OVCAR4, and KURAMOCHI cell lines). Cell viability was assessed by Sulforhodamine B (SRB) colorimetric assay as previously described [28]. Plates were read at 505 nm on a Biotek Synergy 2 Multi-Modal microplate reader (Biotek Instruments Inc., Winooski, Vermont, USA) and data generated using Gen5 imager software (Biotek Instruments Inc., Winooski, Vermont, USA).

#### 2.7. siRNA screening strategy

Lipofectamine® RNAiMAX reagent (Invitrogen, Thermo Fisher Scientific, Loughborough, UK) was used according to the manufacturer's specifications. Cells were seeded at a density of  $3\text{--}5 \times 10^5$  cells in a 20  $\text{cm}^2$  tissue culture dish and underwent validation assay after 72 h incubation unless otherwise stated.

#### 2.8. RT-qPCR methodology

The RealTime® ready Human Reference Gene Panel (Roche, West Sussex, UK) consists of 19 pretested, ready-to-use RT-qPCR reference gene assays along with three positive and two negative control assays for the reverse transcription (RT) reaction preloaded to a 96-well plate. The panel was applied to the study cell model, in accordance with the manufacturers' guidance, to determine the most appropriate reference genes for gene expression assays. The resultant data was then interrogated using the NormFinder version 2.0 algorithm (NormFinder, Department of Molecular Medicine, Aarhus University Hospital, Aarhus, Denmark). All RT-qPCR assays were performed using LightCycler® 480 SYBR Green I Master (Roche, West Sussex, UK), in line with manufacturers' instructions, on the LightCycler® 96 real-time PCR system. For each target of interest, a set of standards, a no treatment control and a non-reverse transcription control were incorporated.

#### 2.9. Western blotting

Briefly, total cellular protein extracts were prepared by adding 200  $\mu\text{L}$  lysis buffer (0.25 M NaCl, 0.1% Igepal, 0.25 M HEPES, 5 mM EDTA, 0.5 mM dithiothreitol [DTT]) to a 90-mm plate containing the relevant cell lines and the lysed cells were harvested with a cell scraper. Each cell lysate was passed through a 21-gauge needle five times, followed by incubation on ice for 10 min to ensure adequate lysis. The lysates were centrifuged at 15000  $g$  for 15 min at 4 °C to pellet the cell debris. The supernatant was stored at  $-20$  °C. Protein concentration in the supernatant was quantified with the use of a Bio-Rad protein assay kit. Equal amounts of protein (typically 60  $\mu\text{g}$  per lane) were analysed by SDS-polyacrylamide gel electrophoresis (PAGE). Following electrophoresis, the proteins were transferred onto Hybond-P polyvinylidene difluoride membrane (Amersham). Transfer was carried out at 100 V for 2 h. Following transfer, the Hybond-P membrane was incubated in blocking solution (5% milk [Marvel] in  $1 \times$  TBST (5 M NaCl, 1 M Tris [pH 7.4], 1 M KCl, 0.1% Tween 20) for 1 h. Primary antibody to RRM2 [1E1] was made up at a concentration of 1:2000 in 5% milk/PBS/T (Abcam, Cambridge, UK). Antimouse was used as secondary at a concentration of 1:2000. The membrane was washed extensively, then subjected to a chemiluminescence detection agent (Amersham) for 5 min. The membrane was then analysed by autoradiography.



## 2.10. Clonogenics

Cells were seeded at a density of  $3 \times 10^5$  per well and forward transfected with two 20 nM RRM2-specific siRNA sequences. Media was replenished after 96 h. Following 7–10 days, colony formation was assessed via crystal violet staining and quantified by resuspension utilising 1 M sodium citrate 50% ethanol solution and absorbance was measured at 570 nm on the Biotrak II microplate reader. Each sample was normalised to the control.

## 2.11. FFPE tissue

All RT-qPCR assays of FFPE-derived cDNA employed the RealTime® Ready platform and pre-amplification (Roche, West Sussex, UK). Pre-amplification with gene-specific primer sets results in >4000-fold amplification of the selected targets without creating a bias towards the original representation of the targets in the input RNA. This technology is ideal for cDNA transcribed from RNA extracted from FFPE tissue. A RealTime® Ready Custom Panel (Roche, UK), comprising 46 targets and 2 controls in duplicate, was designed specifically for this study. The assays were performed in line with the manufacturers' guidance with an input of 200 ng cDNA.

## 2.12. Calculation of relative gene expression

Relative gene expression was calculated from the mean RT-qPCR cycle threshold (CT) data using a standard  $\Delta\Delta CT$  calculation.

## 2.13. Statistical analysis

Analyses were performed using GraphPad Prism version 5 software (La Jolla, California, USA) unless otherwise stated. Statistical tests are indicated in the relevant figure legend alongside p values.

## 3. Results

Gene expression profiling was performed for the following: normal OSE [2], normal fallopian tube epithelium FTE [6], STIC [6], ovarian HGSC (HGSC) [6], and omental metastases (OMT) [6]. Initial unsupervised analysis revealed that the tumour samples (HGSC and OMT) clustered in one cohort, except for one HGSC sample (HGSC\_6) (Fig. 1A & B). Every normal FTE samples clustered together and separately from the normal OSE samples, suggesting a different underlying molecular profile. Notably, the normal OSE samples clustered separately from all other profiled samples, further suggesting a distinct genetic profile. STIC samples clustered within the tumour cohort; interspersed between the HGSC and OMT samples, suggesting that STIC lesions have a common molecular profile to HGSC.

The data were also analysed via correspondence analysis (CA). This agreed with unsupervised clustering analysis in that STIC, HGSC and OMT clustered together; further suggesting a common underlying molecular biology (Fig. 1C & D). Finally, to affirm the likely evolutionary pathway of HGSC, a multi-dimensional scaling analysis was carried out, for both the whole sample set and the top 20% most variant probes (Figs. 1E & F). It confirmed the strong common biology present between STIC and the two tumour groups (HGSC and OMT). It also affirmed the OSE has no significant common genetic biology to the other samples. Having demonstrated

the evolutionary relationship of the samples, we examined changes in gene expression to further clarify the biological pathways driving disease.

Supervised clustering was performed using the top 100 most differentially expressed probes between the three tissue types; normal FTE, STIC and HGSC (Fig. 2). The derived heatmap identified two distinct probeset clusters; one over-expressed in STIC and the other over-expressed in HGSC. These comparisons suggest an evolutionary trajectory from normal FTE to STIC to HGSC, but also further evidence of the significant genetic heterogeneity displayed by HGSC as the disease develops.

Comparison of the top 500 differentially expressed probesets of FTE vs. HGSC, FTE vs. STIC, STIC vs. HGSC, and HGSC vs. OMT (see Supplementary files 4–7) revealed no specific genes common to all four comparisons (see Supplementary file 8). However, there are 43 transcripts common to the FTE vs. HGSC and FTE vs. STIC comparison and 14 transcripts common to the FTE vs. HGSC and the STIC vs. HGSC comparison. Four of these common genes (*ANLN*, *BUB1*, *POLQ*, and *TOP2A*) were selected for validation (Fig. 3A–D). A two-part RT-PCR strategy was used for validation. This involved target screening in both the in vitro model and the Study Cohort FFPE patient samples (Fig. 3E & F respectively). The in vitro model comprised OVCAR4 and KURAMOCHI cell lines to represent HGSC. It also included immortalised fallopian tube epithelial cell lines, FT190 and FT246, used to represent normal FTE and STIC respectively. Samples were normalised to normal FTE or FT190. In this model it is clear there is a significant overexpression of these targets, in both STIC (FT246) and HGSC (OVCAR4 & KURAMOCHI), compared to normal FTE (FT190) (Fig. 3E). Whilst there is also evidence overexpression within the patient samples, most of the targets displayed increased expression in the STIC compared to the HGSC (Fig. 3F).

Using Ingenuity Pathway Analysis (IPA®) (QIAGEN, Redwood City, USA) the top ten canonical pathways for each comparison were identified (Fig. 4). The transformation from normal FTE to STIC is characterised by significant upregulation of mitotic pathways and cyclin activity in regulation of the cell cycle (Fig. 4A). Whereas the transition from STIC to primary HGSC is characterised by upregulation of thrombin, cardiac hypertrophy, and Rho GTPase signalling pathways and pro-survival, pro-angiogenic signals in ovarian HGSC (Fig. 4B). HGSC to OMT transition, representing distant metastatic spread, was characterised by upregulation of immune-related pathways (Fig. 4C).

A careful review of the differentially expressed probesets, and the pathway analysis, identified the most differentially expressed genes (DEGs) that represent high grade serous carcinogenesis (Table 1). Mitosis is enhanced as STIC evolves from normal FTE (*BUB1* and *AURKB*). Pro-inflammatory, pro-invasion, and angiogenic biology becomes more prominent in the STIC to HGSC transition (*ELK1*, *CLNS1A*, and *CADPS*). Finally, upregulation of immune-related, cell adhesion, cell migration, and apoptotic pathways occurs within the metastatic HGSC phase (*CD36*, *ADIPOQ*, and *FABP4*).

To evaluate the functional role of genes in the evolution of normal FTE to STIC a potential oncogene panel was formulated from the top DEGs of the FTE vs. STIC comparisons. An esiRNA approach was then used to identify novel oncogenes driving STIC using viability as a readout. One novel oncogene, involved in cell cycle, mitotic, and metabolism related pathways, that appeared

**Fig. 1.** Unsupervised hierarchical clustering shows two distinct groups (A), when filtered for the top 20% most variant probesets there is evidence that STIC samples hold a common genetic profile to the HGSC and OMT samples (B). The CA confirms the STIC samples to have a common molecular biology with the primary and metastatic HGSC samples in the unsupervised (C) and top 20% filtered (D) datasets, and MDS further emphasises that normal FTE and OSE are distinctly different molecularly but that STIC samples cluster within both HGSC and FTE cohorts in both the unsupervised (E) and top 20% filtered (F) datasets.

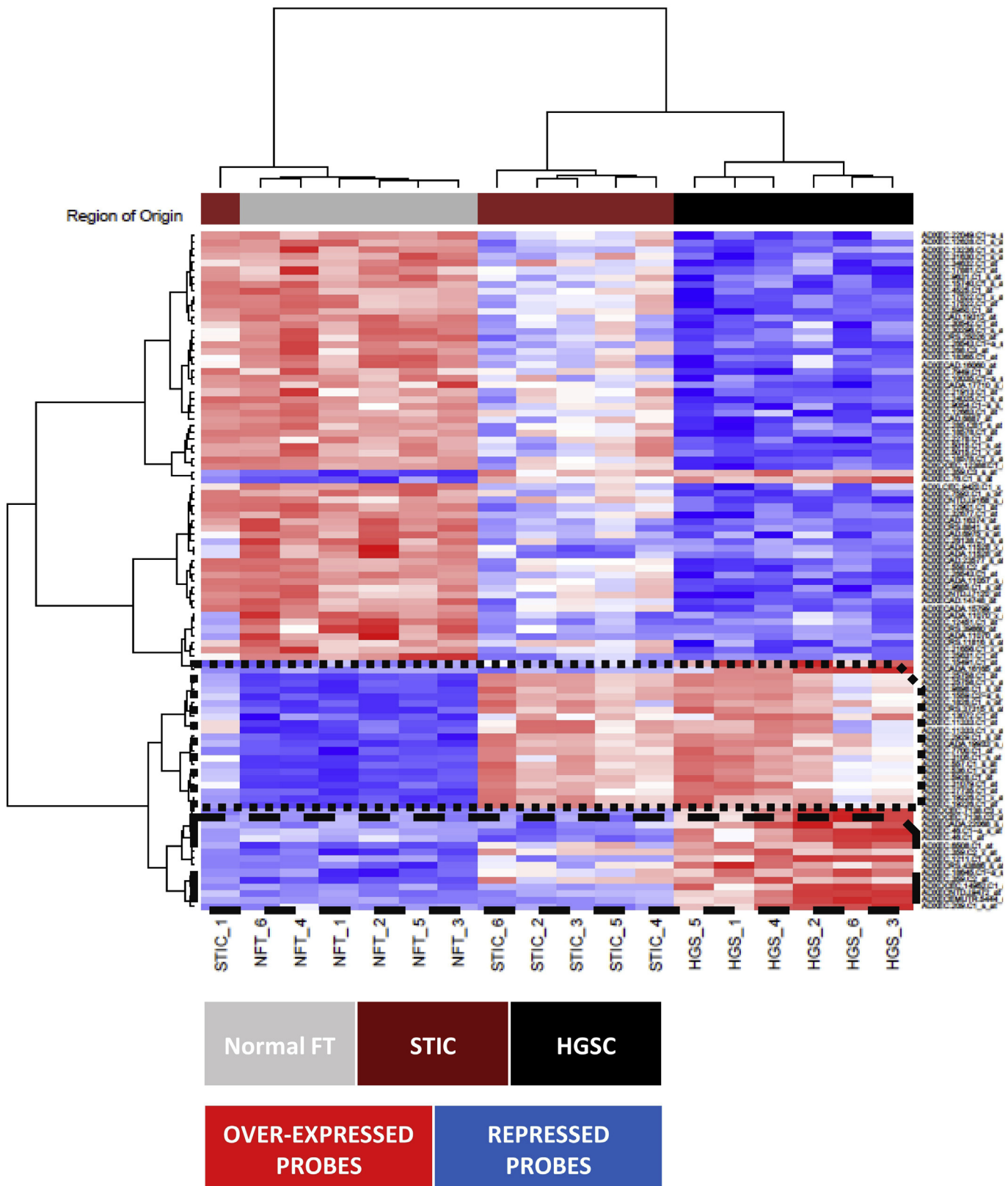


**Fig. 2.** Heatmap showing how the top 100 probesets stratify the three contrasts: Normal FTE, STIC, and HGSC. There appears to be a set of probes becoming progressively repressed and a set progressively over-expressed from normal FTE to HGSC, via STIC. Within the set of probes that become over-expressed with HGSC, a subgroup appears to be over-expressed with the development of STIC (dotted box) whereas another subgroup appears to delay over-expression until the development of HGSC (dashed box).

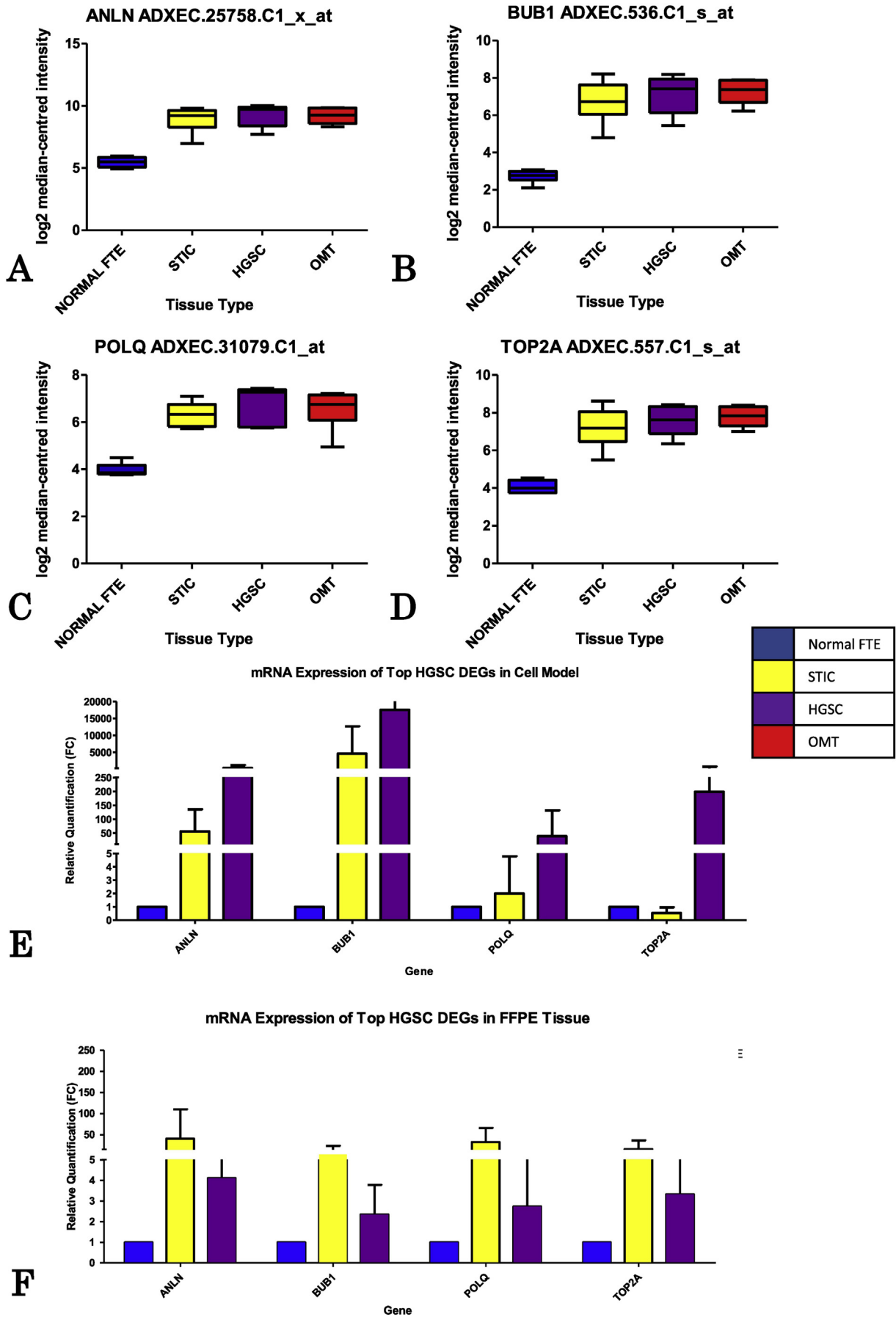


**Fig. 3.** Four transcripts selected for validation of the GEP array (A–D). All show a fold change of 2–3 between normal FTE and “Cancer”. Again, STIC samples behave molecularly similarly to primary HGSC. Unpaired *t*-test confirms statistical significance between normal FTE and any other tissue type with a *p*-value consistently <0.005. The four transcripts were interrogated by RqPCR within the HGSC-specific cell model (E) and within the FFPE-tissue samples (F).

consistently was *Ribonucleotide Reductase M2 (RRM2)* (Fig. 5). The screen also confirmed the crucial role of many of the mitotic genes (e.g. *ANLN*, *BUB1B* and *TOP2A*) that were previously shown to be overexpressed in STIC and HGSC (Fig. 3A–F). The role of RRM2 was further explored using independent siRNAs in both the HGSC-specific cell model and also a non-HGSC ovarian cancer cell panel. The loss of RRM2 clearly had an effect on cell growth but it did not appear to be HGSC-specific (Fig. 6A–D). At a protein level, examined by western blot, there was no demonstrable effect of RRM2 silencing (Fig. 6E & F). These data suggest RRM2 may play a role in EOC carcinogenesis but is not specific to HGSC.

During this project a study using similar samples was published [29]. This provided us with a unique opportunity to use these additional samples as a validation cohort. They reported a common molecular profile of STIC and invasive STIC (HGSC) with evidence of a 62-gene signature that becomes overexpressed with carcinogenesis. When the 62-gene signature was applied to our independent cohort similar results were noted (see Supplementary file 9). The normal FTE cluster is distinctly separate from that of the STIC and HGSC. The outcome of this analysis reinforces the strength of the current study's GEP dataset but also further emphasises the HGSC evolution from normal FTE.

#### 4. Discussion

There is an ever-expanding body of pathological evidence supporting the fallopian tube as the site of origin of extrauterine HGSC. The majority of the initial evidence emanated from the study of RRSO specimens from women at high risk of developing HGSC [13]. Since then, evidence has accumulated that sporadic HGSCs also derive from the fallopian tube in a significant majority of cases [30]. The current study adds weight to the pathological evidence by defining the underlying molecular profile of HGSC. Specifically, it provides molecular evidence of the evolution of HGSC from the fallopian tube with STIC as a transition point.

The comparison of the top 500 differentially expressed probe-sets of FTE vs. HGSC, FTE vs. STIC, STIC vs. HGSC, and HGSC vs. OMT proved interesting. The fact there were specific groups of genes common to the FTE vs. HGSC and FTE vs. STIC comparison and the STIC vs. HGSC and FTE vs. HGSC comparison suggests these clusters of genes may be associated with the malignant transformation of normal FTE. Furthermore, the fact most genes associated with distant metastatic spread (HGSC vs OMT) are not common with any other group suggests they are associated disease survival and metastases rather than cancer initiation.

The observation of upregulated mitotic genes and aberrant cell cycle regulators in the evolution of normal FTE to STIC advances the relative paucity of knowledge regarding early HGSC carcinogenesis. The surge of mitotic pathway expression and cyclin activity combined with reciprocal repression of cell cycle checkpoint regulation (particularly in association with DNA damage) is both in keeping with the genomic instability of HGSC and characteristic of this phase of disease pathogenesis. One study reported cell cycle arrest and increased expression of the mitotic checkpoint members in a cell model designed to mimic STIC lesions as they aged in culture [31]. Concurrently, it was shown that down-regulation of *BRCA1* in the aging cells led to activation of the anaphase promoting complex and subsequent return to the cell growth pattern seen with 'younger' cells. It is likely that loss of *BRCA1* may lead to initiation of a new cell cycle without full completion of cytokinesis. This biology is classical of an early carcinogenic event and carries significant potential for biomarker and therapeutic development.

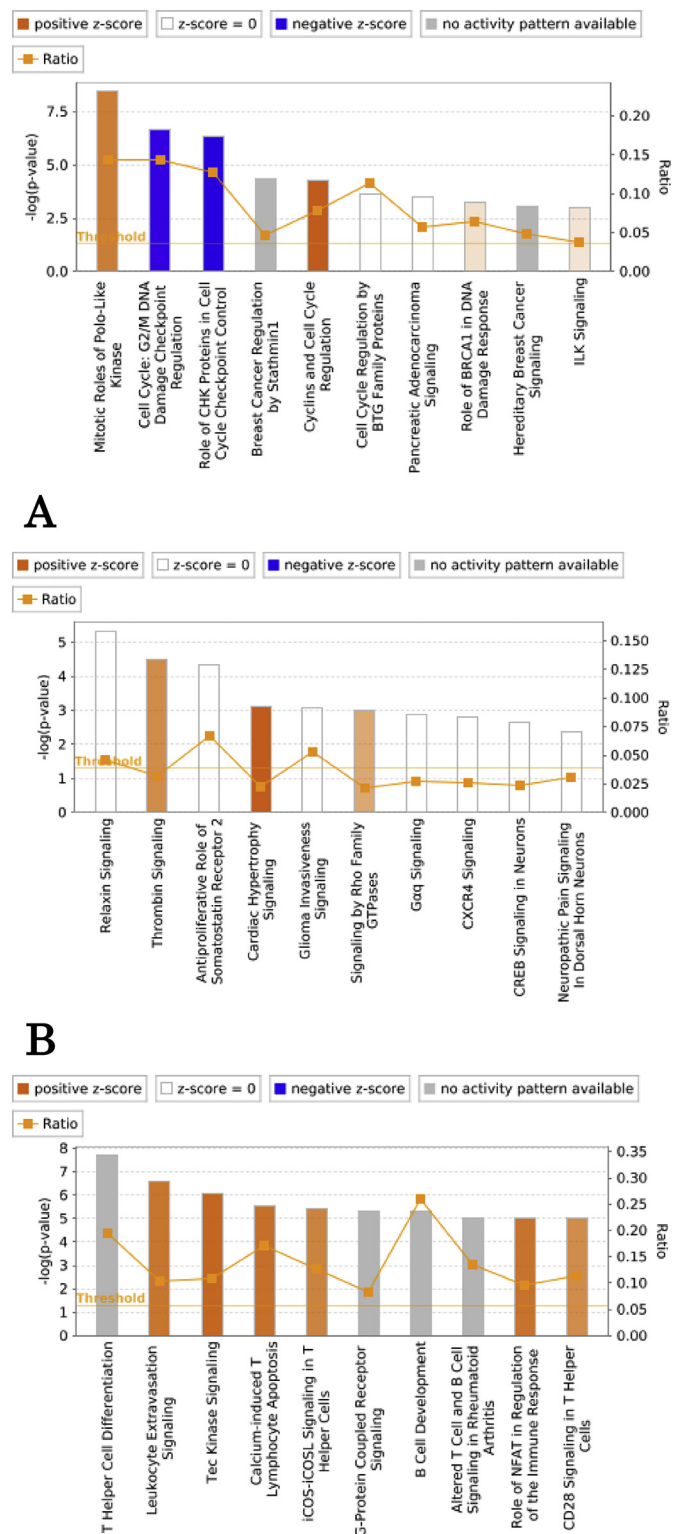


**Fig. 4.** IPA® reveals the top 10 canonical pathways associated with the progression from normal FTE to STIC (A), STIC to HGSC (B), and HGSC to Omental Metastases (OMT) (C). The analysis assessed the activity of canonical pathways within the dataset, based on the z-score. An orange bar means the analysis software predicted an overall increase in the activity of the pathway, a blue bar means the software predicted an overall decrease in the activity of the pathway, a white bar means the z-score was close to zero (and activity therefore unchanged from normal) and a grey bar means that activity "predictions" weren't possible (mainly due to a lack of publications in the topic area). The ratio of pathway activity is marked by the orange line. (For interpretation of the references to color in this figure legend, the reader is referred to the web version of this article.)

The molecular profile of the STIC to HGSC transition is characterised by upregulation of thrombin, cardiac hypertrophy, and Rho GTPases signalling pathways. This stage of pathogenesis is associated with early intraperitoneal metastasis and other groups have reported elevated thrombin signalling, with downstream upregulation of *NF- $\kappa$ B*, and pro-inflammatory platelet activation mediating cell invasion and pro-survival, pro-angiogenic signals in ovarian cancer cells [32]. The role of Rho family GTPases and their downstream effectors, like ROCK and ERK, have also been shown to play a major role in epithelial – mesenchymal transition, cancer cell motility, and invasion in ovarian cancer [33,34].

The evolution of HGSC to OMT is characterised by upregulation of immune-related pathways. Leucocyte extravasation signalling upregulation associated with elevated Rho GTPase activity has been reported in the STIC to HGSC transition [35]. It also plays a role in transition of leucocytes from the bloodstream to tissue and vice versa; this is an important feature of metastases and potentially could be manipulated for liquid biopsies. Elevated Tec Kinase signalling also correlates with this stage of disease, as it is an activator of adhesion, migration, apoptosis, and a known T-cell activator. Similarly, iCOS-iCOSL signalling is heavily involved with T-helper cell activation and differentiation via *NFAT* signalling. These findings are in keeping with the knowledge of the role of immune evasion in the survival of a range of cancers [36]. The DEG pathway analysis of ovarian to omental HGSC transition in our study reflects a state of immune dysregulation (notably via T-helper lymphocyte and B-lymphocyte regulated genes), indicating processes such as T-Cell exhaustion which has been reported to be a feature of advanced HGSC [37]. Therapeutically, this could indicate this late stage of disease might be vulnerable to immune checkpoint-based therapies.

Whilst this study is based upon a limited sample set, it is uniquely suited to carefully analyse alterations in pathology as the data arises from samples from the same patient. This reduces the experimental noise that would normally be associated with inter-patient comparisons. Accurate, detailed pathological annotation and expansive gene expression profiling further amplify the quality of the resulting data. Although only two normal OSE samples were included in the study due to quality control constraints, there was a clear separation of these samples from all other samples included in the study. Furthermore, given the evidence that STIC has a common molecular profile to HGSC (both ovarian and omental), the wealth of prior pathological evidence suggesting STIC is the primary neoplasm, and the fact that STIC lesions originate on the distal FTE, this study provides further support for a fallopian tubal origin for HGSC.

Additional support for the fallopian origin comes from combined analysis between this study and a prior study [29]. There are no other studies that have compared ovarian tumour/HGSC with normal fallopian tube. To date, expression profiling studies of ovarian carcinogenesis continue to use OSE as a comparator-control [38]. This external dataset also identified mitotic genes, as in the current study, to be overexpressed in early carcinogenesis, again suggesting that mitotic dysfunction is crucial to the evolution of HGSC. The combined analysis validated the strength of our gene expression profiling dataset with the normal FTE vs. STIC signature clearly separating the normal FTE from the ‘cancer’ cluster. The same effect was not seen for the STIC vs. HGSC signature and this may reflect the slight difference in tissue source or the loss of gene classifiers on transfer between analysis platforms. The fact that the biological profile of early carcinogenesis seen in this study was confirmed in the combined analysis affirms the scientific approach of using the fallopian tube, rather than normal OSE as in previous studies, as the comparator cell of origin. Consequently, this bolsters

**Table 1**

The most differentially expressed genes associated with evolution of the high grade serous carcinoma. Each set of genes is an indicative reflection of the underlying molecular biology within each phase.

NFT-STIC
<i>TPX2, Microtubule-Associated (TPX2)</i>
<i>Budding Uninhibited By Benzimidazoles 1 (BUB1)</i>
<i>Ubiquitin-Conjugating Enzyme E2C (UBE2C)</i>
<i>Anillin Actin Binding Protein (ANLN)</i>
<i>Aurora Kinase B (AURKB)</i>
<i>Abnormal Spindle Microtubule Assembly (ASPM)</i>
<i>Ligand Dependent Nuclear Receptor Corepressor-Like (LCORL)</i>
<i>ZW10 Interacting Kinetochore Protein (ZWINT)</i>
STIC-HGSC
<i>Delta-Like 1 Homolog (DLK1)</i>
<i>Kelch Domain Containing 8A (KLDCH8A)</i>
<i>Chloride Channel, Nucleotide-Sensitive, 1A (CLNS1A)</i>
<i>ELK1, Member of ETS Oncogene Family (ELK1)</i>
<i>Calcium-Dependent Secretion Activator (CADPS)</i>
<i>Collectin Sub-family Member 11 (COLEC11)</i>
<i>TraB Domain Containing 2A (TRAB2A)</i>
HGSC-OMT
<i>Adiponectin, C1Q and Collagen Domain Containing (ADIPOQ)</i>
<i>CD36 Molecule (Thrombospondin Receptor) (CD36)</i>
<i>Fatty Acid Binding Protein 4, Adipocyte (FABP)</i>
<i>Delta-Like 1 Homolog (DLK1)</i>
<i>Kelch Domain Containing 8A (KLDCH8A)</i>
<i>Collectin Sub-family Member 11 (COLEC11)</i>
<i>Perilipin 1 (PLIN1)</i>
<i>Alcohol Dehydrogenase 1B (class I), Beta Polypeptide (ADH1B)</i>

the molecular evidence of a carcinogenic pathway from normal FTE to HGSC, via STIC.

## 5. Conclusion

The characterisation of the underlying molecular profile of HGSC has more clearly defined the evolutionary trajectory of the disease. Consequently, it adds to the current body of knowledge regarding disease pathogenesis. The identification of key regulatory pathways, most notably the aberrant upregulation of mitosis-related pathways, has also provided insight into the biological processes driving the evolution of HGSC from the fallopian tube. The understanding of the biology of this disease is crucial to the development of both novel interventions and disease-specific biomarkers. Therapeutic agents targeting key regulatory pathways carry significant promise for future treatments of HGSC but the key to the reduction in mortality from HGSC is the identification of a highly sensitive, disease-specific screening biomarker. However, in the interim, we would advocate the opportunistic surgical removal of fallopian tubes when a woman has completed her family as another approach that could significantly reduce the incidence of this devastating disease [39,40].

Supplementary data to this article can be found online at <https://doi.org/10.1016/j.ygyno.2019.08.029>.

## Acknowledgments

We firstly want to acknowledge the valuable contributions made by our late colleague Dr. Jennifer Quinn-O'Brien who was instrumental in the design and initiation of this project. The Gene

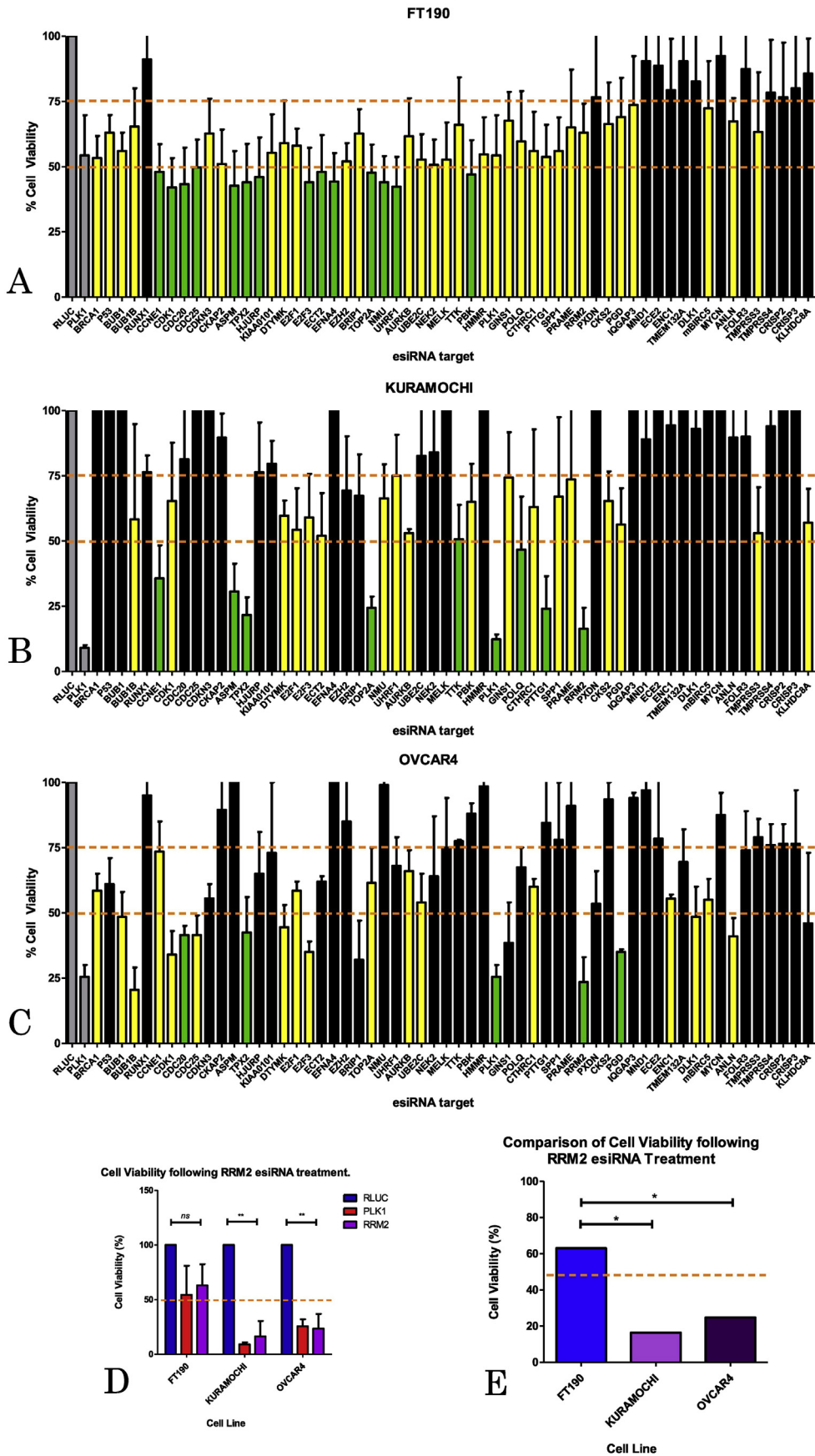


**Fig. 5.** Mission esiRNA screen of 58 oncogenes in the HGSC cell model (A–C). The dashed red lines represent 75% and 50% cell viability thresholds, while the yellow and green bars represent targets that displayed cell viability below those respective thresholds ( $n = 3$ ). esiRNA knockdown of RRM2 had a significantly greater negative effect on cell viability in KURAMOCHI ( $p = 0.009$ ) and OVCAR4 ( $p = 0.006$ ) than FT190 ( $p = 0.08$ ) (D). Comparison of the negative effect on cell viability showed a significant difference between both FT190 and KURAMOCHI ( $p = 0.04$ ) and FT190 and OVCAR4 ( $p = 0.02$ ) (E). (For interpretation of the references to color in this figure legend, the reader is referred to the web version of this article.)

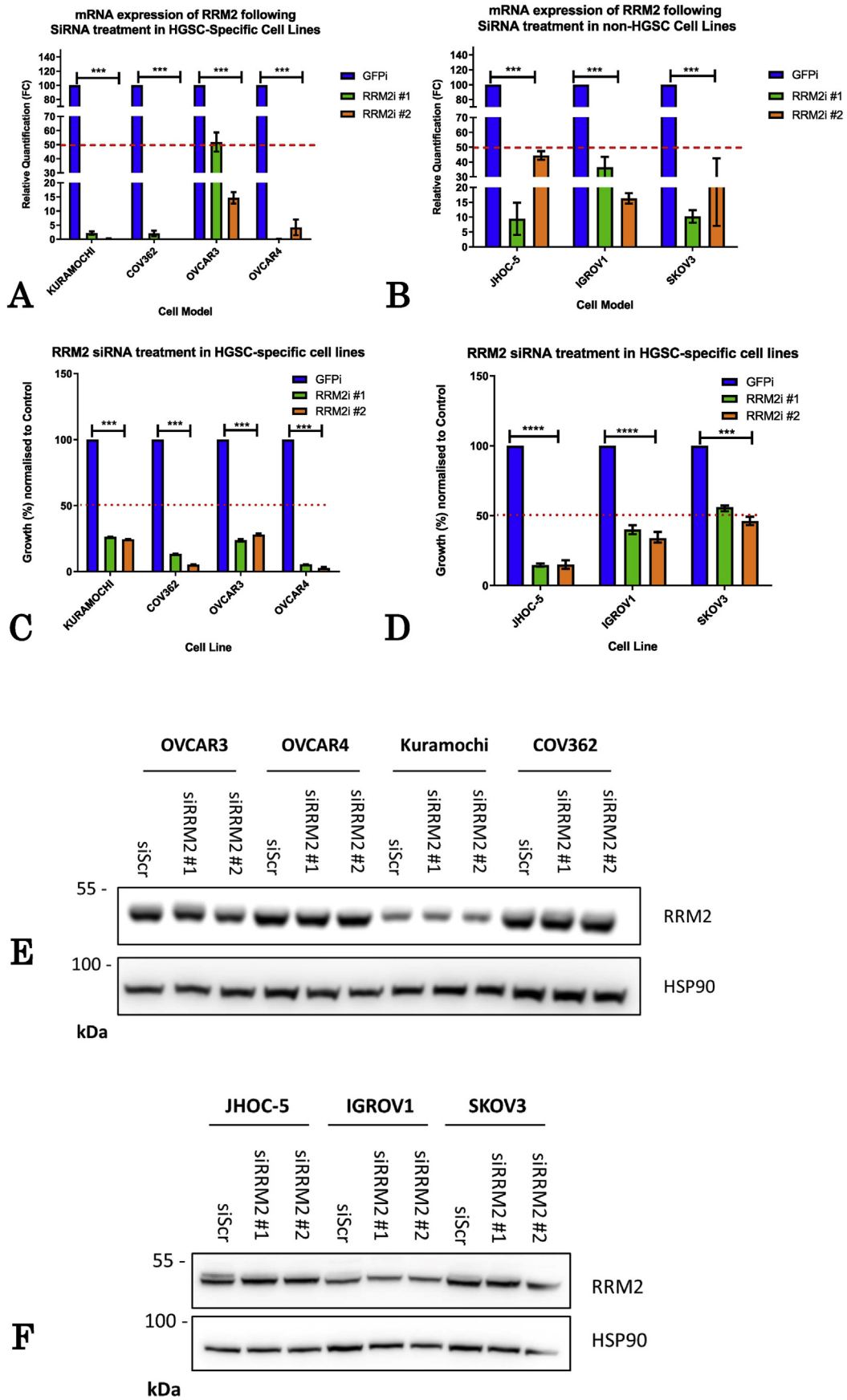


**Fig. 6.** Validation with two independent siRNAs for RRM2 in the HGSC cell model and the non-HGSC cell panel confirm RRM2 knockdown has a negative effect on cell growth ( $p < 0.005$ ) (A-D). Assessment, by western blotting, of protein expression reveals RRM2 knockdown does not translate at a protein level (E & F).

Expression Profiling data from this study would not have been possible without the generous support of the Belfast Health and Social Care Trust Samaritan Fund. The samples used in this research were received from the Northern Ireland Biobank which is funded by HSC Research and Development Division of the Public Health Agency in Northern Ireland and Cancer Research UK through the Belfast CRUK Centre and the Northern Ireland Experimental Cancer Medicine Centre; additional support was received from the Friends of the Cancer Centre. The Northern Ireland Molecular Pathology Laboratory, which is responsible for creating resources for the NIB, has received funding from Cancer Research UK, the Friends of the Cancer Centre and the Sean Crummey Foundation. The research fellowship of the lead author (JPB) was also funded by HSC Research and Development Division of the Public Health Agency in Northern Ireland.

#### Author contributions

The study was conceived, designed and initiated by JPB, IJGH, WGM, and PBM through the Ovarian Cancer Research Focus Group at CCRCB, QUB. IJGH and WGM selected appropriate cases through the Northern Ireland Centre for Gynaecological Cancer Multidisciplinary Meeting. WGM performed pathological analysis and annotation. JPB collated all relevant clinico-pathological data. DMcA, AR, AG, PO, PD, NM, NB provided bioinformatics support and were involved in analysis of the raw gene expression profiling (GEP) data. MST provided support for tissue sectioning and annotation through the Northern Ireland Molecular Pathology Laboratory. RDK and NM provided support for GEP assay. MST, RD and RDK were also invaluable in results analysis and interpretation. RID supplied fallopian tube cells for in vitro assays. JPB, CM, DLE, JF, PC and LF did all laboratory validation work with support from PBM, SLE and NB. JPB and PBM prepared the manuscript. All authors were involved in refining and finalising the manuscript for submission.

#### Declaration of competing interest

Professor Richard Kennedy is Vice President and Medical Director of Almac Diagnostics, ALMAC, Craigavon, UK. Dr. Nuala McCabe is an employee of Almac Diagnostics, ALMAC, Craigavon, UK. Professor Ronny Drapkin serves on the scientific advisory board of Repare Therapeutics, Siamab Therapeutics, and Pear Tree Therapeutics.

#### References

- [1] CRUK, Ovarian Cancer. <http://www.cancerresearchuk.org/health-professional/cancer-statistics/statistics-by-cancer-type/ovarian-cancer>, 2014. (Accessed April 2016).
- [2] A.A. Ahmed, D. Etemadmoghadam, J. Temple, et al., Driver mutations in TP53 are ubiquitous in high grade serous carcinoma of the ovary, *J. Pathol.* 221 (2010) 49–56.
- [3] J.P. Beirne, G.W. Irwin, S.A. McIntosh, I.J.G. Harley, D.P. Harkin, The molecular and genetic basis of inherited cancer risk in gynaecology, *The Obstetrician & Gynaecologist* 17 (2015) 233–241.
- [4] C. Gourley, C.O. Michie, P. Roxburgh, et al., Increased incidence of visceral metastases in Scottish patients with BRCA1/2-defective ovarian cancer: an extension of the ovarian BRCAness phenotype, *J. Clin. Oncol.* 28 (2010) 2505–2511.
- [5] J.I. Weberpals, K.V. Clark-Knowles, B.C. Vanderhyden, Sporadic epithelial ovarian cancer: clinical relevance of BRCA1 inhibition in the DNA damage and repair pathway, *J. Clin. Oncol.* 26 (2008) 3259–3267.
- [6] D.D. Bowtell, The genesis and evolution of high-grade serous ovarian cancer, *Nat. Rev. Cancer* 10 (2010) 803–808.
- [7] M.F. Fathalla, Incessant ovulation—a factor in ovarian neoplasia? *Lancet* 2 (1971) 163.
- [8] A.S. Whittemore, R. Harris, J. Itnyre, Characteristics relating to ovarian cancer risk: collaborative analysis of 12 US case-control studies. IV. The pathogenesis of epithelial ovarian cancer. Collaborative Ovarian Cancer Group, *Am. J. Epidemiol.* 136 (1992) 1212–1220.
- [9] K.A. Rosenblatt, D.B. Thomas, Lactation and the risk of epithelial ovarian cancer. The WHO Collaborative Study of Neoplasia and Steroid Contraceptives, *Int. J. Epidemiol.* 22 (1993) 192–197.
- [10] H.O. Adami, C.C. Hsieh, M. Lambe, et al., Parity, age at first childbirth, and risk of ovarian cancer, *Lancet* 344 (1994) 1250–1254.
- [11] H.A. Risch, L.D. Marrett, G.R. Howe, Parity, contraception, infertility, and the risk of epithelial ovarian cancer, *Am. J. Epidemiol.* 140 (1994) 585–597.
- [12] N. Singh, W.G. McCluggage, C.B. Gilks, High-grade serous carcinoma of tubo-ovarian origin: recent developments, *Histopathology* 71 (2017) 339–356.
- [13] J.M.J. Piek, P.J. van Diest, R.P. Zweemer, et al., Dysplastic changes in prophylactically removed fallopian tubes of women predisposed to developing ovarian cancer, *J. Pathol.* 195 (2001) 451–456.
- [14] A. Finch, P. Shaw, B. Rosen, J. Murphy, S.A. Narod, T.J. Colgan, Clinical and pathologic findings of prophylactic salpingo-oophorectomies in 159 BRCA1 and BRCA2 carriers, *Gynecol. Oncol.* 100 (2006) 58–64.
- [15] Y. Lee, A. Miron, R. Drapkin, et al., A candidate precursor to serous carcinoma that originates in the distal fallopian tube, *J. Pathol.* 211 (2007) 26–35.
- [16] E. Kuhn, R.J. Kurman, R. Vang, et al., TP53 mutations in serous tubal intra-epithelial carcinoma and concurrent pelvic high-grade serous carcinoma—evidence supporting the clonal relationship of the two lesions, *J. Pathol.* 226 (2012) 421–426.
- [17] L. Gautier, L. Cope, B.M. Bolstad, R.A. Irizarry, affy-analysis of Affymetrix GeneChip data at the probe level, *Bioinformatics* 20 (2004) 307–315.
- [18] Team RC, R: A Language and Environment for Statistical Computing, R Foundation for Statistical Computing, Vienna, Austria, 2012.
- [19] S. Dray, A.B. Dufour, The ade4 package: implementing the duality diagram for ecologists, *J. Stat. Softw.* 22 (2007) 1–20.
- [20] A.C. Culhane, J. Thioulouse, G. Perriere, D.G. Higgins, MADE4: an R package for multivariate analysis of gene expression data, *Bioinformatics* 21 (2005) 2789–2790.
- [21] R. Gentleman, V. Carey, W. Huber, F. Hahne, Genefilter: Genefilter: Methods for Filtering Genes From High-throughput Experiments. R Package, 2015 (1.52.0).
- [22] F. Murtagh, P. Legendre, Ward's hierarchical agglomerative clustering method: which algorithms implement ward's criterion? *J. Classif.* 31 (2014) 274–295.
- [23] A. Day, heatmap.plus: Heatmap With More Sensible Behavior, 29/10/2012, <http://CRAN.R-project.org/package=heatmap.plus>, 2012. (Accessed 20 November 2015).
- [24] M.E. Ritchie, B. Phipson, D. Wu, et al., limma powers differential expression analyses for RNA-sequencing and microarray studies, *Nucleic Acids Res.* 43 (2015) e47.
- [25] Anglesio MSW, K. C.; Melnyk, N.; Chow, C.; Salamanca, C.; Prentice, L. M.; Senz, J.; Wang, W.; Spillman, M. A.; Cochrane, D. R.; Shumansky, K.; Shah, S. P.; Kalloger, S. E.; Huntsman, D. G. Type-specific cell line models for type-specific ovarian cancer research. *PLoS One* 2013; 8.
- [26] S. Domcke, R. Sinha, D.A. Levine, C. Sander, N. Schultz, Evaluating cell lines as tumour models by comparison of genomic profiles, *Nat. Commun.* 4 (2013) 2126.
- [27] A.M. Karst, R. Drapkin, Primary culture and immortalization of human fallopian tube secretory epithelial cells, *Nat. Protoc.* 7 (2012) 1755–1764.
- [28] V. Vichai, K. Kirtikara, Sulforhodamine B colorimetric assay for cytotoxicity screening, *Nat. Protoc.* 1 (2006) 1112–1116.
- [29] Y. Yamamoto, G. Ning, B.E. Howitt, et al., In vitro and in vivo correlates of physiological and neoplastic human fallopian tube stem cells, *J. Pathol.* 238 (2016) 519–530.
- [30] C.B. Gilks, J. Irving, M. Kobel, et al., Incidental nonuterine high-grade serous carcinomas arise in the fallopian tube in most cases: further evidence for the tubal origin of high-grade serous carcinomas, *Am. J. Surg. Pathol.* 39 (2015) 357–364.
- [31] V.M. Yu, C.M. Marion, T.M. Austria, J. Yeh, A.H. Schonthal, L. Dubeau, Role of BRCA1 in controlling mitotic arrest in ovarian cystadenoma cells, *Int. J. Cancer* 130 (2012) 2495–2504.
- [32] K. Egan, D. Crowley, P. Smyth, et al., Platelet adhesion and degranulation induce pro-survival and pro-angiogenic signalling in ovarian cancer cells, *PLoS One* 6 (2011), e26125.
- [33] Z.Z. Pan, W. Bruening, A.K. Godwin, Involvement of RHO GTPases and ERK in synuclein-gamma enhanced cancer cell motility, *Int. J. Oncol.* 29 (2006) 1201–1205.
- [34] J. Peng, G. Zhang, Q. Wang, et al., ROCK cooperated with ET-1 to induce epithelial to mesenchymal transition through SLUG in human ovarian cancer cells, *Biosci. Biotechnol. Biochem.* 76 (2012) 42–47.

- [35] N. Heemskerk, J. van Rijssel, J.D. van Buul, Rho-GTPase signaling in leukocyte extravasation: an endothelial point of view, *Cell Adhes. Migr.* 8 (2014) 67–75.
- [36] D.S. Vinay, E.P. Ryan, G. Pawelec, et al., Immune evasion in cancer: mechanistic basis and therapeutic strategies, *Semin. Cancer Biol.* 35 (2015), S185–S198.
- [37] K. Abiko, M. Mandai, J. Hamanishi, et al., PD-L1 on tumor cells is induced in ascites and promotes peritoneal dissemination of ovarian cancer through CTL dysfunction, *Clin. Cancer Res.* 19 (2013) 1363–1374.
- [38] L. Zhang, M. Luo, H. Yang, S. Zhu, X. Cheng, C. Qing, Next-generation sequencing-based genomic profiling analysis reveals novel mutations for clinical diagnosis in Chinese primary epithelial ovarian cancer patients, *J. Ovarian Res.* 12 (2019) 19.
- [39] J.S. Kwon, Ovarian cancer risk reduction through opportunistic salpingectomy, *J. Gynecol. Oncol.* 26 (2015) 83–86.
- [40] RCOG, The Distal Fallopian Tube as the Origin of Non-uterine Pelvic High-grade Serous Carcinomas, Royal College of Obstetricians and Gynaecologists, 2014.